Encoding technique for design of zero-order (on-axis) Fraunhofer computer-generated holograms

David Mendlovic, Gal Shabtay, Uriel Levi, Zeev Zalevsky, and Emanuel Marom

Diffractive optical elements able to generate zero-order (on-axis) distributions with phase as well as amplitude distributions are described. The proposed elements are surface relief plates, i.e., phase-only elements, that are based on the concept of computer-generated masks followed by common etching processes. The encoding method assumes fixed spatial partitioning of the cell and a phase-only value allocated to each subelement. The reconstructed amplitude and phase distributions contain imperfections (noise) resulting from the encoding process. Methods of error reduction and improvements are provided. © 1997 Optical Society of America

1. Introduction

Holography has played a major role in optical data processing.[1,2] The common method use for displaying complex function was by means of modulating the spatial information on a carrier signal. In optics this consisted of a modulated grating. The reconstruction displayed the desired function along the first diffraction order (off-axis holography). Methods of synthetic generation of holographic elements were first introduced by Brown and Lohmann[3] and Lohmann and Paris,[4] who invented the first computerized encoding method for holograms. The computer-generated holograms produced by this approach were binary and were allowed to yield desired complex function distributions at arbitrary planes along the direction of the first diffraction order.

For far-field reconstructions, the Fourier transform of the desired distribution to be reconstructed is evaluated at discrete cell locations called pixels. In one implementation, the amplitude of each pixel is encoded by the plotting of a binary square inside the area of the hologram's pixel. The normalized area of the plotted square is inversely proportional to the amplitude to be encoded in that pixel, while the out-of-center position of the square within the pixel is used to encode the phase. Different encoding procedures were later suggested by Lee,[5] Burckhart,[6] Hsueh and Sawchuck,[7] Gallagher and Bucklew,[8] and Matic and Hensen.[9] In each approach a specific mathematical relation that connects the out-of-center location and the area of a blocking pattern (commonly square) to the phase and the amplitude, respectively, to be encoded has been derived. A common feature of all these methods is that the reconstructed image is displayed along the first order of diffraction, and the conjugated image is obtained along the opposite order.

One of the main disadvantages of obtaining a reconstruction along the first diffraction order is that the reconstruction accuracy is highly dependent on the illumination wavelength. If deviation of the wavelength λ occurs in the illumination source, as often happens in practical optical systems with commonly available light sources, the quality of reconstruction rapidly decreases with the amount of deviation. Moreover, working along the first diffraction order increases the complexity of the system, does not allow on-line operation, and often decreases significantly the light efficiency of the system.

In view of the above, zero-order encoding methods might yield superior performances. The main drawback of these methods is that the implementation of zero-order holograms is in general more difficult because it requires several etching steps if one desires nonbinary operation. Nevertheless, owing to rapid developments in microelectronics, in recent years improvement in etching accuracy has developed rapidly and thus fabrication of many etching depth levels is easy to achieve through, for example, controlling the coating deposition thickness. Therefore lately the implementation of zero-order holograms has become much more feasible.

The history of phase-only diffractive optical elements (kinoforms) was initiated in 1969 by Lesem

The authors are with the Faculty of Engineering, Tel-Aviv University, 69978 Tel-Aviv, Israel.

Received 10 February 1997; revised manuscript received 30 May 1997.

0003-6935/97/328427-08$10.00/0

et al.[10] Their approach for encoding phase-only information was to modulate a sawtooth phase structure. The periodic structure generates a beam in the direction of the first diffraction order, which carries the phase information by virtue of the modulation introduced on the sawtooth grating. In this approach the amplitude information of the wave front is assumed to be constant on the basis of the assumption that, for the reconstruction, the phase information of a wave front is much more significant than the amplitude information. Horner and Leger[11] too analyzed the behavior of phase-only elements when they are used as matched filters in correlation setups.

The assumption that phase information is more important than amplitude information does not hold for all cases. Indeed, an improvement to the kinoform approach that also enables the encoding of amplitude information has been suggested by Kirk and Jones.[12] According to their method, the reconstructed image is obtained in any desired order, including zero diffraction order, by modulating the amplitude information on a high-frequency phase carrier that diffracts the undesired light into higher orders. However, the spatial frequency needed to encode the amplitude should be high so that errors are reduced. Therefore, in addition to the high-phase resolution (etching depth resolution) needed to encode the phase, this method also requires high spatial resolution to handle the amplitude information.

A simplification of this method was suggested by Florence and Juday.[13] In their approach the amplitude information is modulated by the division of each pixel, now designated macropixel, into only two equal subpixels with a different phase allocated to each subpixel. A limited spatial resolution is now needed, however, for this encoding procedure results in a very large error.

We investigate variations of these encoding techniques that are able to produce a much better performance. In Section 2 this approach is analyzed in detail for the first time. This analysis is necessary for estimating the relatively large error terms, as derived in Section 3, in the reconstructed image. Section 4 presents modifications that provide major improvements to the basic approach and significantly reduce the error factors while the required spatial resolution is kept relatively low. Computer simulations that prove the capability of the proposed encoding approaches are shown in Section 5.

2. Encoding Procedure

The basic zero-order phase-only encoding procedure as shown by Florence and Juday[13] is based on regarding the mask plane as being composed of macropixels. Each macropixel consists of two equal regions, each region manufactured (etched) in a way such that it displays a uniform phase value. The aim of the subdivision is the encoding of amplitude as well as phase information by phase-only elements. Therefore the procedure described relies on using pure phase-only functions that may be fabricated with techniques such as plasma etching and chemical etching, among others. The obtained resulting beam is generated with relatively high light efficiency. Moreover those devices can be replicated with ease and are cost effective. The encoding approach requires spatial resolution lower than that needed for conventional first-order elements because the encoded free parameters are the phases etched in each one of the partitions rather than the locations. The required amplitude and phase of each cell (macropixel) converts into a specific phase value that is assigned to each cell's partition (pixel).

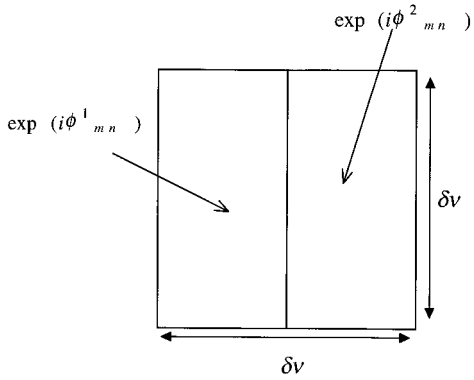

Fig. 1. Top view of one cell (m, n).

A two-dimensional top view construction of the basic encoding cell elements (m, n) is illustrated in Fig. 1, and a typical etching profile is shown schematically in Fig. 2. Each cell in this basic representation is encoded through two sections of equal widths. Two free parameters exist in this representation: $\phi^{(1)}_{m,n}$ and $\phi^{(2)}_{m,n}$ (shown in Fig. 2), which are the phases etched in each one of the two partitions of the cell (m, n). These free parameters are shown to produce the necessary phase and the amplitude encoding of that cell. The mathematical expression for the filter represented by all cells is given by

$$
\begin{aligned}
H(\nu_x, \nu_y) = \sum_m \sum_n \operatorname{rect}\left(\frac{\nu_y}{\delta\nu}\right)\operatorname{rect}\left(\frac{2\nu_x}{\delta\nu}\right) \\
* \left(\exp(i\phi^{(1)}_{m,n})\left\{\delta\left[\nu_x - \left(m + \frac{1}{4}\right)\delta\nu\right]\right.\right. \\
\left.\times \delta\left[\nu_y - \left(n + \frac{1}{2}\right)\delta\nu\right]\right\} + \exp(i\phi^{(2)}_{m,n}) \\
\left.\times \delta\left[\nu_x - \left(m + \frac{3}{4}\right)\delta\nu\right]\delta\left[\nu_y - \left(n + \frac{1}{2}\right)\delta\nu\right]\right),
\end{aligned}
\tag{1}
$$

where $*$ denotes convolution, $\delta\nu$ is the lateral dimension of the pixel, and δ is the Dirac impulse function.

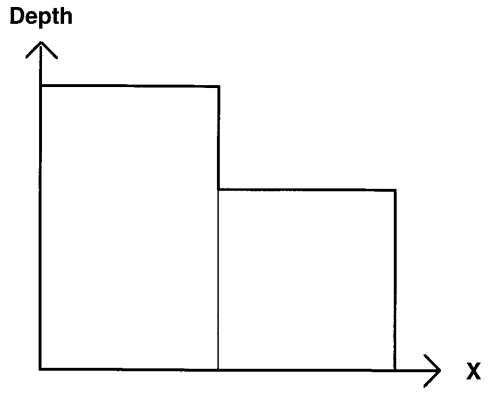

Fig. 2. Etching profile of cell (m, n).

Let $h(x, y)$ be the inverse Fourier transform of $H(\nu_x, \nu_y)$. We then have

$$h(x, y) = \int_{-\infty}^{\infty} \int_{-\infty}^{\infty} H(\nu_x, \nu_y) \exp[i2\pi(x\nu_x + y\nu_y)] \mathrm{d}\nu_x \mathrm{d}\nu_y. \tag{2}$$

Thus one obtains

$$h(x, y) = \frac{\delta\nu^2}{2} \exp\left(i2\pi y \frac{\delta\nu}{2}\right) \exp\left(i2\pi x \frac{\delta\nu}{4}\right) \mathrm{sinc}\left(\frac{\delta\nu x}{2}\right) \times \mathrm{sinc}(\delta\nu y) \sum_m \sum_n \left[\exp(i\phi_{m,n}^{(1)}) + \exp(i\phi_{m,n}^{(2)}) \times \exp\left(i2\pi x \frac{1}{2} \delta\nu\right)\right] \exp[i2\pi\delta\nu(xm + yn)], \tag{3}$$

where $\mathrm{sinc}(x)$ is defined as

$$\mathrm{sinc}(x) = \frac{\sin(\pi x)}{\pi x}. \tag{4}$$

Because the inverse Fourier transform of the encoded function is displayed along the zero diffraction order, we restrict our interest to regions of (x, y) corresponding to $x, y \ll 1/\delta\nu$. Therefore

$$\delta\nu x \ll 1, \qquad \delta\nu y \ll 1, \tag{5}$$

and, as a result,

$$\mathrm{sinc}(\delta\nu x), \mathrm{sinc}(\delta\nu y) \approx 1, \qquad \exp(i2\pi x\delta\nu), \exp(i2\pi y\delta\nu) \approx 1. \tag{6}$$

Equation (3) now becomes

$$h(x, y) \approx \frac{\delta\nu^2}{2} \sum_m \sum_n [\exp(i\phi_{m,n}^{(1)}) + \exp(i\phi_{m,n}^{(2)})] \times \exp[i2\pi\delta\nu(xm + yn)]. \tag{7}$$

In a discrete system, the filter $H(\nu_x\nu_y)$ should represent an arbitrary complex distribution that in cell (m, n) is given by

$$H(m\delta\nu, n\delta\nu) = A_{m,n} \exp(i\phi_{m,n}). \tag{8}$$

The Fourier integral of Eq. (2) is then transformed to a summation:

$$h(x, y) \approx (\delta\nu)^2 \sum_m \sum_n H(m\delta\nu, n\delta\nu) \times \exp[i2\pi(xm + yn)\delta\nu]. \tag{9}$$

The expression in the left-hand square brackets of expression (7) can be mathematically manipulated to provide

$$h(x, y) = (\delta\nu)^2 \sum_m \sum_n \cos\left(\frac{\phi_{m,n}^{(1)} - \phi_{m,n}^{(2)}}{2}\right) \times \exp\left(i \frac{\phi_{m,n}^{(1)} + \phi_{m,n}^{(2)}}{2}\right) \exp[i2\pi(xm + yn)\delta\nu]. \tag{10}$$

If we normalize the amplitude values such that $0 \leq A_{m,n} \leq 1$, a comparison between expression (9) and Eq. (10) yields that the amplitude and the phase of each cell are determined uniquely by the values of $\phi_{m,n}^{(1)}$ and $\phi_{m,n}^{(2)}$ so that

$$A_{m,n} = \cos\left(\frac{\phi_{m,n}^{(1)} - \phi_{m,n}^{(2)}}{2}\right), \tag{11}$$

$$\phi_{m,n} = \left(\frac{\phi_{m,n}^{(1)} + \phi_{m,n}^{(2)}}{2}\right). \tag{12}$$

Hence, if the samples of the Fourier transform of the desired image are given by the discrete values $H(m\delta\nu, n\delta\nu)$ as defined in Eq. (8), then $\phi_{m,n}^{(1)}$ and $\phi_{m,n}^{(2)}$ should satisfy the following equations:

$$\phi_{m,n}^{(1)} = \phi_{m,n} + \cos^{-1}(A_{m,n}), \tag{13}$$

$$\phi_{m,n}^{(2)} = \phi_{m,n} - \cos^{-1}(A_{m,n}). \tag{14}$$

Note that the above-described method reconstructs the Fourier transform of the encoded function along the optical axis, in the zero-diffraction-order direction. However, the approach can be applied to other optical transformations as well. For example, the reconstruction might be applied over the Fresnel transform or the fractional Fourier transform of the encoded function with exactly the same encoding procedure. In addition, this method is appropriate also for holography, i.e., image plane reconstruction.

3. Error Terms

The main cause for performance reduction of the encoding method of Section 2 is that there is a spatial shift between the two different phases that encode the amplitude and the phase of each cell. If the two phases could be superposed, there might be less performance reduction. It is well known that the Fourier transform of a shifted object contains an additional linear phase factor. This phase is the term $\exp[i2\pi x(\delta\nu/2)]$, multiplying $\exp(i\phi_{m,n}^{(2)})$ in Eq. (3). Best performance would be obtained if the terms that multiply $\exp(i\phi_{m,n}^{(1)})$ and $\exp(i\phi_{m,n}^{(2)})$ would

be as similar as possible. Such would be the case if an interferometric setup, whereby each cell would be composed of two superimposed phase functions, would be possible. The implementation and the alignment requirements of such a setup are prohibitive. If this does not happen, a distorted image will indeed be obtained. As an example, assume $A_{m,n} = 1$ and $\phi_{m,n} = 0$ for every (m, n). According to Eqs. (13) and (14), $\phi^{(1)}_{m,n} = \phi^{(2)}_{m,n} = 0$. The reconstructed object $h(x, y)$ [see Eq. (3)] is expected within the window $|x|\delta\nu \le 1/2$. At the center x = 0, we indeed obtain

$$\exp\left(i2\pi x\,\frac{\delta\nu}{2}\right) = 1,$$

$$\frac{\exp(i\phi^{(1)}_{m,n}) + \exp\left(i2\pi x\,\frac{\delta\nu}{2}\right)\exp(i\phi^{(2)}_{m,n})}{2} = 1, \quad (15)$$

which is fine, but at the edge for $X = 1/2\delta\nu$ we obtain

$$\exp\left(i2\pi x\,\frac{\delta\nu}{2}\right) = i,$$

$$\frac{\exp(i\phi^{(1)}_{m,n}) + \exp\left(i2\pi x\,\frac{\delta\nu}{2}\right)\exp(i\phi^{(2)}_{m,n})}{2} = \frac{1+i}{2}, \quad (16)$$

which provides a rather large error. As one can see, the error is a function of the x coordinate. At $x = 0$ there is no error and at $x = 1/2\delta\nu$ the error is maximal. To estimate the error, one should define an accuracy predictor (AP), which is the ratio of the coefficients of $\exp(i\phi^{(1)}_{m,n})$ and $\exp(i\phi^{(2)}_{m,n})$ in Eq. (3), which results in

$$\mathrm{AP} = \exp\left(i2\pi x\,\frac{\delta\nu}{2}\right). \quad (17)$$

|AP| should be as close as possible to 1, and its phase should be close to zero to achieve the same contribution from those two terms everywhere. Without any corrections, we have just seen that at $x = 1/2\delta\nu$ we obtain AP = i. As we discussed, such an error is large and should be reduced.

4. Error Reduction Schemes

We describe several ways for reducing the effect of these errors and analyze their effect.

A. Oversampling

We considered sampling the hologram (Fourier transform information) at a rate higher than the minimum necessary one (Shannon rate). The best practical way to increase the sampling is to surround the original object with zeros, which is equivalent to reducing the incremental frequency step $\delta\nu$ after the Fourier transform operation. Let the original object size be $u_{\max}$; the added strip of zeros increases it to $U_{\max}$. The new incremental frequency step $\delta\nu$ is $1/U_{\max}$. The oversampling factor P is defined as:

$$P = \frac{U_{\max}}{u_{\max}}. \quad (18)$$

The reconstructed image will have a size $U_{\max}$. However, the interest is restricted to the $u_{\max}$ so that $X_{\max}$ in Eq. (17) is now restricted to $X_{\max} = u_{\max}/2 = 1/\delta\nu u_{\max}$, and the AP is at the limit portion of the image:

$$\mathrm{AP} = \exp\left(i2\pi X_{\max}\,\frac{\delta\nu}{2}\right) = \exp\left(i2\pi\,\frac{1}{4P}\right).$$

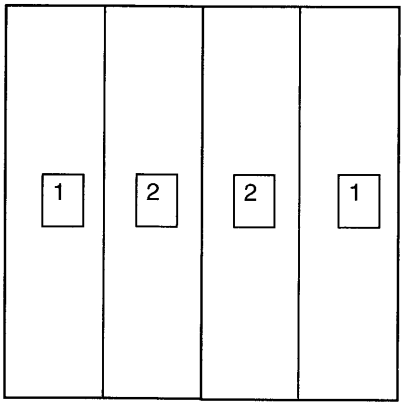

Fig. 3. Top view of one cell; 1-D symmetrical structure.

B. One-Dimensional Symmetric Partition

Instead of dividing the cell into two fixed partitions (which is an asymmetrical structure), we propose to divide the cell into four fixed partitions, which allows allocating the two phase values in a symmetric fashion (see Fig. 3). The value of the two inner partitions is determined to be $\exp(i\phi^{(2)}_{m,n})$, whereas the value of the two outer partitions is set to $\exp(i\phi^{(1)}_{m,n})$. Such a filter is accordingly represented by

$$\begin{aligned} H(\nu_x, \nu_y) = \sum_m \sum_n & \mathrm{rect}\left(\frac{\nu_y}{\delta\nu}\right)\mathrm{rect}\left(\frac{4\nu_x}{\delta\nu}\right) \\ & * \left(\exp(i\phi^{(1)}_{m,n})\left\{\delta\left[\nu_x - \left(m + \frac{1}{8}\right)\delta\nu\right]\right.\right. \\ & \left. + \delta\left[\nu_x - \left(m + \frac{7}{8}\right)\delta\nu\right]\right\} + \exp(i\phi^{(2)}_{m,n}) \\ & \left.\times\left\{\delta\left[\nu_x - \left(m + \frac{3}{8}\right)\delta\nu\right] + \delta\left[\nu_x - \left(m + \frac{5}{8}\right)\delta\nu\right]\right\}\right) \\ & \times \delta\left[\nu_y - \left(n + \frac{1}{2}\right)\delta\nu\right]. \end{aligned} \quad (19)$$

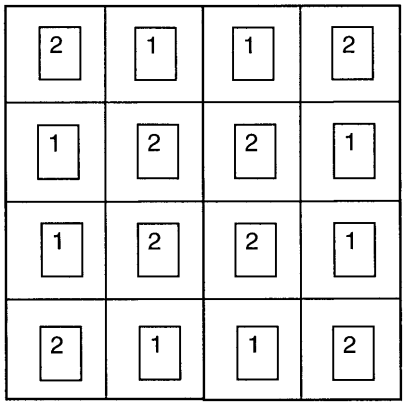

Fig. 4. Top view of one cell; 2-D symmetrical structure.

The distribution of the reconstructed beam is thus given by

$$h(x,y) = \frac{(\delta\nu)^2}{4}\exp\left(i2\pi y\frac{\delta\nu}{2}\right)\exp\left(i2\pi x\frac{\delta\nu}{2}\right)\mathrm{sinc}\left(\frac{\delta\nu x}{4}\right) \times \mathrm{sinc}(\delta\nu y)\sum_m\sum_n\left\{\exp(i\phi^{(1)}_{m,n}) \times\left[\exp\left(-i2\pi\frac{3}{8}\delta\nu\right)+\exp\left(i2\pi\frac{3}{8}\delta\nu\right)\right] + \exp(i\phi^{(2)}_{m,n})\left[\exp\left(-i2\pi x\frac{1}{8}\delta\nu\right) + \exp\left(i2\pi\frac{1}{8}\delta\nu\right)\right]\right\}\exp[i2\pi\delta\nu(xm+yn)]. \tag{20}$$

Rearranging the elements of Eq. (20) and using approximation (6), one obtains

$$h(x,y) \approx \frac{(\delta\nu)^2}{2}\sum_m\sum_n\left[\exp(i\phi^{(1)}_{m,n})\cos\left(2\pi x\frac{3}{8}\delta\nu\right) + \exp(i\phi^{(2)}_{m,n})\cos\left(2\pi x\frac{1}{8}\delta\nu\right)\right] \times \exp[i2\pi\delta\nu(xm+yn)]. \tag{21}$$

Combining the one-dimensional (1-D) symmetric structure approach with the oversampling approach described in Section 3 results in better accuracy. The AP at the image edge, where the error is at the maximum level, is given by

$$\mathrm{AP} = \frac{\cos(\pi/8p)}{\cos(3\pi/8p)}. \tag{22}$$

For example, using the symmetrical code $p = 4$, one gets AP = 1.04. For a fair comparison with the asymmetric approach, one should use $p = 8$ because the symmetric approach needs twice the resolution of the asymmetric approach. One then obtains that AP for that asymmetric approach is AP = $\exp[i(\pi/16)] = 0.98 + 0.19i$, which is worse than the one evaluated for the symmetric case because of the complex value.

C. Two-Dimensional Symmetric Structure

The 1-D symmetric structure can be expanded into a two-dimensional (2-D) symmetric structure as shown in Fig. 4. The filter is now

$$H(\nu_x,\nu_y) = \sum_m\sum_n \mathrm{rect}\left(\frac{4\nu_y}{\delta\nu}\right)\mathrm{rect}\left(\frac{4\nu_x}{\delta\nu}\right) * \left[\left(\exp(i\phi^{(1)}_{m,n})\left\{\delta\left[\nu_x-\left(m+\frac{1}{8}\right)\delta\nu\right] + \delta\left[\nu_x-\left(m+\frac{7}{8}\right)\delta\nu\right]\right\} + \exp(i\phi^{(2)}_{m,n}) \times\left\{\delta\left[\nu_x-\left(m+\frac{3}{8}\right)\delta\nu\right] + \delta\left[\nu_x-\left(m+\frac{5}{8}\right)\delta\nu\right]\right\}\right) \times\left\{\delta\left[\nu_y-\left(m+\frac{3}{8}\right)\delta\nu\right] + \delta\left[\nu_y-\left(m+\frac{5}{8}\right)\delta\nu\right]\right\} + \left(\exp(i\phi^{(2)}_{m,n}) \times\left\{\delta\left[\nu_x-\left(m+\frac{1}{8}\right)\delta\nu\right]+\delta\left[\nu_x-\left(m+\frac{7}{8}\right)\delta\nu\right]\right\} + \exp(i\phi^{(1)}_{m,n})\left\{\delta\left[\nu_x-\left(m+\frac{3}{8}\right)\delta\nu\right] + \delta\left[\nu_x-\left(m+\frac{5}{8}\right)\delta\nu\right]\right\}\right)\left\{\delta\left[\nu_y-\left(m+\frac{1}{8}\right)\delta\nu\right] + \delta\left[\nu_y-\left(m+\frac{7}{8}\right)\delta\nu\right]\right\}\right]. \tag{23}$$

Considerations the same as in Eqs. (20) and (21) lead to

$$h(x,y) \approx \frac{(\delta\nu)^2}{2}\sum_m\sum_n\left\{\exp(i\phi^{(1)}_{m,n})\left[\cos\left(2\pi x\frac{3}{8}\delta\nu\right) \times\cos\left(2\pi y\frac{1}{8}\delta\nu\right)+\cos\left(2\pi x\frac{1}{8}\delta\nu\right)\cos\left(2\pi y\frac{3}{8}\delta\nu\right)\right] + \exp(i\phi^{(2)}_{m,n})\left[\cos\left(2\pi x\frac{3}{8}\delta\nu\right)\cos\left(2\pi y\frac{3}{8}\delta\nu\right) + \cos\left(2\pi x\frac{1}{8}\delta\nu\right)\cos\left(2\pi y\frac{1}{8}\delta\nu\right)\right]\right\} \times\exp[i2\pi\delta\nu(xm+yn)]. \tag{24}$$

A combination of the 2-D symmetric approach with the above oversampling conclusion results in

$$\mathrm{AP} = \frac{\cos(3\pi/8p)+\cos(\pi/8p)}{2\cos(3\pi/8p)\cos(\pi/8p)}. \tag{25}$$

Table 1. Accuracy Predictor for Basic Approach, Including Improvements

P	Basic Approach	1-D Structure	2-D Structure
1	$1 < \frac{\pi}{2}$	2.41	1.84
2	$1 < \frac{\pi}{4}$	1.17	1.11
4	$1 < \frac{\pi}{8}$	1.04	1.02
8	$1 < \frac{\pi}{16}$	1.01	1
16	$1 < \frac{\pi}{32}$	1	1

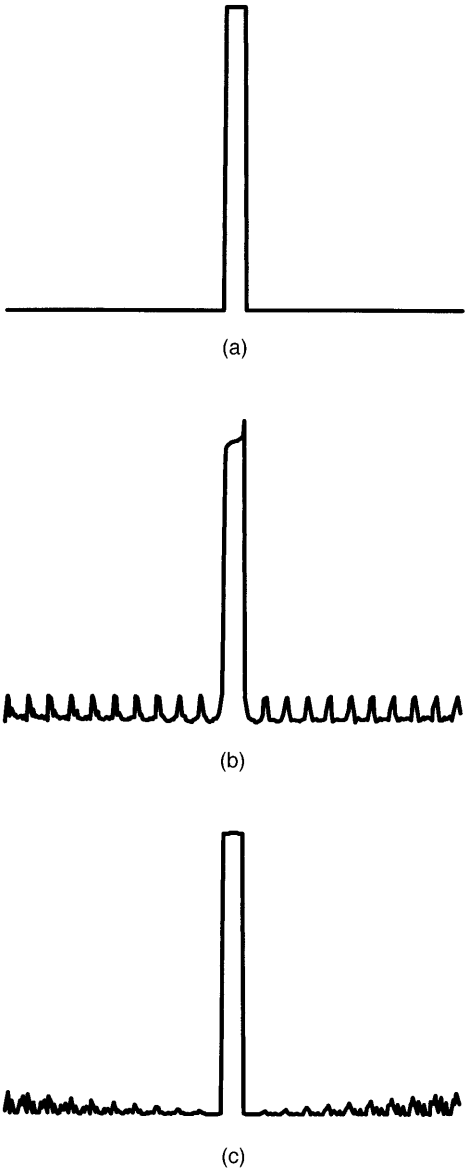

Fig. 5. (a) 1-D top-hat object to be encoded, (b) obtained reconstruction for original method, (c) obtained reconstruction using 1-D symmetrical structure.

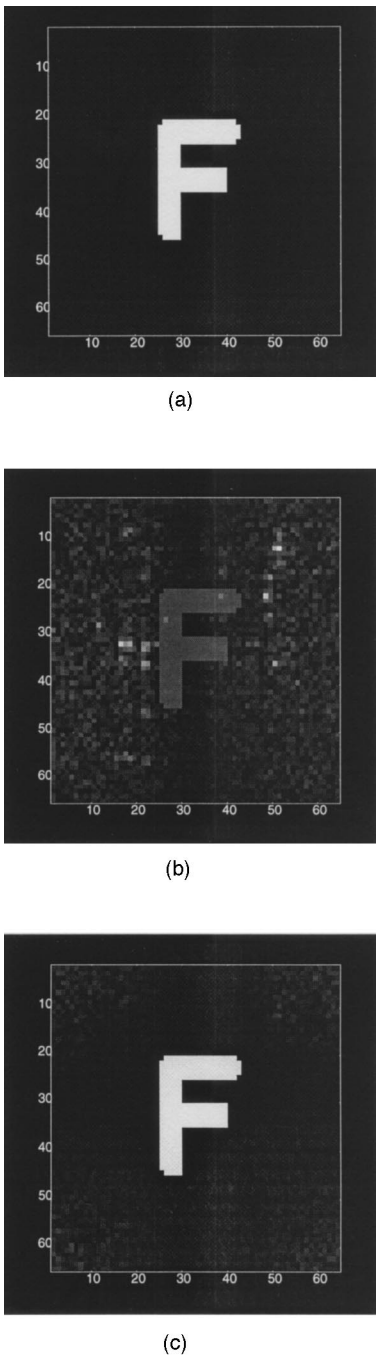

Fig. 6. (a) 2-D image to be encoded, (b) obtained reconstruction for original method, (c) obtained reconstruction using 2-D symmetrical structure.

For example, for $P = 2$ Eq. (25) indicates that AP = 1.11 while for the 1-D symmetric structure AP is 1.17 [see Eq. (22)]. Moreover, the basic encoding method (asymmetric approach) results in AP = $0.92 + 0.38i$. The superiority of the 2-D symmetric structure is evident.

Table 1 provides a summary of the expected performances of the basic approach and its two improvement variations, expressed by the AP. One can see that the AP for the basic approach is a complex num-

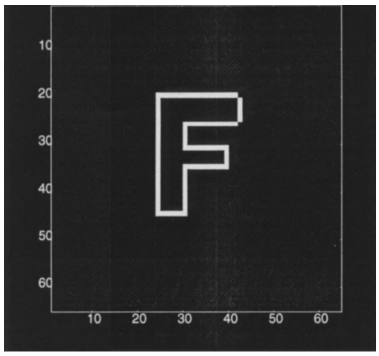

(a)

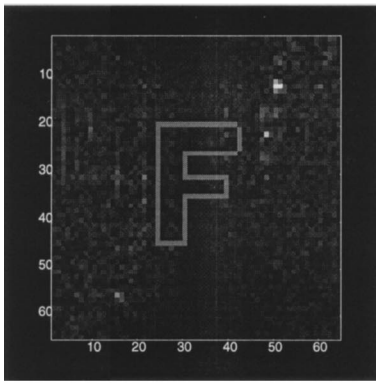

(b)

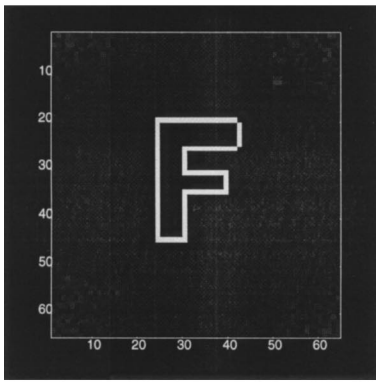

(c)

Fig. 7. (a) 2-D image to be encoded, (b) obtained reconstruction for original method, (c) obtained reconstruction using 2-D symmetrical structure.

ber while the AP for the symmetrical approach is real. The complex number represents a phase error, which might be more dangerous than an amplitude error in the reconstruction plane. It is also evident from this table that for a given value of p the accuracy predictor achieved by the 2-D structure is better than that achieved by the 1-D structure.

5. Computer Simulations

To demonstrate the capabilities of the proposed zero-order encoding method, we carried out computer simulations. Figure 5(a) shows a 1-D top-hat (box) object that was encoded with the two-fixed-partitions method. The zero-order region of the output plane is shown in Fig. 5(b) (for $p = 40$). Figure 5(c) shows the same region achieved with the 1-D symmetric structure approach (for $p = 20$). One can see that the quality of the reconstruction is good and that high uniformity is achieved.

To test the method on 2-D images, we present a 2-D image in Fig. 6(a). Figure 6(b) is the obtained reconstruction around the zero order achieved by the encoding of the image using the two-fixed-partitions method ($p = 4$). Figure 6(c) shows the same region achieved with the 2-D symmetric structure approach ($p = 2$). Figure 7(a) is the outline of Fig. 6(a). The same reconstruction is shown again in Figs. 7(b) and 7(c). Once again the reconstruction is good and unblurred, i.e., the high frequencies were resolved.

6. Conclusions

Approaches for encoding arbitrary phase and amplitude distributions are proposed. The suggested methods are based on phase-only filter (produced by a plasma etching device), thus resulting in relatively high light efficiency. The hologram mask was designed to reconstruct around the zero order of diffraction and therefore is insensitive to variations in the wavelength of the illuminating source. The suggested implementation is suited for high-resolution phase-etching production and low spatial resolution, while a previous described approach (Ref. 12) requires both spatial resolution and depth resolution to be high. Thus this approach offers great potential for dynamic elements that are based on spatial light modulators. The obtained elements are ready to replace the binary amplitude computer-generated holograms in a variety of applications such as optical correlators, displays, beam shaping devices, and so forth. Computer simulations have shown that the methods can cope successfully in reconstructing different types of objects and have emphasized the better reconstruction results achieved by those methods in comparison with the other phase-only zero-order hologram approaches.

References

1. J. W. Goodman, *Introduction to Fourier Optics* (McGraw-Hill, San Francisco, 1968).
2. A. Vander Lugt, "Signal detection by complex spatial filtering," IEEE Trans. Inf. Theory **IT-10,** 139–146 (1964).
3. B. R. Brown and A. W. Lohmann, "Complex spatial filtering with binary masks," Appl. Opt. **5,** 967–969 (1966).
4. A. W. Lohmann and D. P. Paris, "Binary Fraunhofer holograms, generated by computer," Appl. Opt. **6,** 1739–1749 (1967).
5. W. H. Lee, "Sampled Fourier transform hologram generated by computer," Appl. Opt. **9,** 639–643 (1970).
6. C. B. Burkhardt, "A simplification of Lee's method of generating holograms by computer," Appl. Opt. **9,** 1949 (1970).
7. C. K. Hsueh and A. A. Sawchuck, "Computer-generated double phase holograms," Appl. Opt. **17,** 3874–3883 (1978).
8. N. C. Gallagher and J. A. Bucklew, "Nondetour phase digital holograms: an analysis: errata," Appl. Opt. **19,** 4266–4272 (1980).

9. R. M. Matic and E. W. Hensen, "Nondetour computer-generated holograms: an improvement variation," Appl. Opt. **21,** 2304–2305 (1982).
10. L. B. Lesem, P. M. Hirsch, and J. A. Jordan, Jr., "The kinoform: a new wavefront reconstruction device," IBM J. Res. Dev. **13,** 150–155 (1969).
11. J. L. Horner and J. R. Leger, "Pattern recognition with binary phase-only filters," Appl. Opt. **24,** 609–611 (1985).
12. J. P. Kirk and A. L. Jones, "Phase-only complex-valued spatial filter," J. Opt. Soc. Am. **61,** 1024–1028 (1971).
13. J. M. Florence and R. D. Juday, "Full-complex spatial filtering with a phase mostly DMD," in *Wave Propagation and Scattering in Varied Media II*, V. K. Varadan, ed., Proc. SPIE **1558,** 487–498 (1991).